

Enhanced magnetorheological effect of suspensions based on carbonyl iron particles coated with poly(amidoamine) dendrons

Citation

PLACHÝ, Tomáš, Martin CVEK, Lukáš MÜNSTER, Barbora HANULÍKOVÁ, Pavol ŠULY, Alenka VESEL, and Qilin CHENG. Enhanced magnetorheological effect of suspensions based on carbonyl iron particles coated with poly(amidoamine) dendrons. In: *Rheologica Acta* [online]. vol. 60, iss. 5, Springer Science and Business Media Deutschland, 2021, p. 263 - 276 [cit. 2022-06-01]. ISSN 0035-4511. Available at <https://link.springer.com/article/10.1007/s00397-021-01269-1>

DOI

<https://doi.org/10.1007/s00397-021-01269-1>

Permanent link

<https://publikace.k.utb.cz/handle/10563/1010286>

Terms of use

Elsevier 2022. This manuscript version is made available under the CC-BY-NC-ND 4.0 license <https://creativecommons.org/licenses/by-nc-nd/4.0/>.

This document is the Accepted Manuscript version of the article that can be shared via institutional repository.



TBU Publications

Repository of TBU Publications

publikace.k.utb.cz

Enhanced magnetorheological effect of suspensions based on carbonyl iron particles coated with poly(amidoamine) dendrons

Tomas Plachy^{a,b*}, Martin Cvek^a, Lukas Munster^a, Barbora Hanulikova^a, Pavol Suly^a, Alenka Vesel^c, Qilin Cheng^{a,b*}

^a*Centre of Polymer Systems, University Institute, Tomas Bata University in Zlin, Trida Tomase Bati 5678, 760 01 Zlin, Czech Republic*

^b*Key Laboratory for Ultrafine Materials of the Ministry of Education, School of Materials Science and Engineering, East China University of Science and Technology, Shanghai 200237, China*

^c*Department of Surface Engineering and Optoelectronics, Jozef Stefan Institute, Jamova cesta 39, 1000 Ljubljana, Slovenia*

*Corresponding authors: e-mail address: plachy@utb.cz (T. Plachy); chengql@ecust.edu.cn (Q. Cheng)

Abstract

Particle oxidation constitutes a serious ageing phenomenon in magnetorheological suspensions, bringing about deterioration in performance. This study describes commercial carbonyl iron particles that were successfully coated with poly(amidoamine) dendrons and then applied as an oxidation-resistant dispersed phase in magnetorheological suspensions. A synthesis method was adhered to whereby the particles were sequentially treated with ethylenediamine and methyl acrylate, leading to the formation of generation 2 and 2.5 dendrons; these had the capacity for composite particles with a nano-scale dendritic layer to be prepared on their surfaces. Success in applying the coating was confirmed by various techniques, including XPS, TEM, EDX, FTIR and Raman spectroscopy. The controlled approach adopted to coating the carbonyl iron particles resulted in them exhibiting sufficient oxidation stability, with only a ~4.5–4.7% decrease in saturation magnetization. Of interest was that their magnetorheological

29 suspensions demonstrated ca 4.8% and 4% higher dynamic yield stress than a suspension based
30 on non-modified particles at the highest intensity of magnetic field investigated, *i.e.* 438 kA m⁻¹.
31 ¹. Notably, sedimentation stability was evaluated by a unique method that involved the use of a
32 tensiometer with a specific testing probe. The aforementioned coating process led to enhanced
33 sedimentation stability of the magnetorheological suspensions based on coated particles
34 possibly due to decrease in the overall density of the particles, enhanced dispersion stability
35 and reduction in the size of their agglomerates in the silicone oil mixtures that were confirmed
36 by optical microscopy. Modification of the particles as proposed has the potential to overcome
37 one of the primary drawbacks of magnetorheological suspensions, this being oxidation
38 instability (which leads to what is referred to as “in-use-thickening”), without negatively
39 affecting their performance in the presence of a magnetic field.

40 **Keywords**

41 Carbonyl iron; magnetorheology; yield stress; sedimentation stability; poly(amidoamine)

42 **Introduction**

43 Magnetorheological (MR) suspensions (MRSs) are intelligent systems whose rheological
44 parameters can be controlled through applying a magnetic field. They are generally composed
45 of a non-magnetic liquid medium and a dispersed phase of magnetic particles, most commonly
46 carbonyl iron particles (CIPs). These otherwise randomly distributed particles create chain-like
47 structures when exposed to a magnetic field (Feijoo et al. 2020, Machovsky et al. 2015, Marins
48 et al. 2019), causing an abrupt rise in viscosity and other rheological parameters of such MRSs
49 (Bell et al. 2008, Bombard et al. 2015, Cvek et al. 2020, De Vicente et al. 2011, Han et al. 2019,
50 Morillas et al. 2018). Behaviour of this type is referred to as the MR effect, which has found
51 numerous industrial applications, including in damping systems, shock absorbers, as a medium
52 in an MR clutch and in MR polishing (Bucchi et al. 2013, Chen et al. 2003, Kwon et al. 2015,
53 Park et al. 2010, Utami et al. 2018, Zhu et al. 2012).

54 A recognized issue affecting MRSs is that during long-term operation they undergo what is
55 referred to as “in-use-thickening” (IUT) (Carlson and Jolly 2000, Utami, Ubaidillah, Mazlan,
56 Imaduddin, Nordin, Bahiuddin, Aziz, Mohamad and Choi 2018). This brings about increase in
57 the resistive force of the instrument, accompanied by the given system showing rise in yield
58 stress values in the absence of a magnetic field (Roupec and Mazurek 2011, Roupec et al. 2013).
59 In-use-thickening is caused by abrasion or delamination of the oxidized layers on the surfaces
60 of CIPs (Ulicny et al. 2007), constituting a primary drawback of MRSs. For example, Ulicny et

61 al. (Ulicny, Balogh, Potter and Waldo 2007) utilized an MRS as an operating medium in an MR
62 clutch. During the investigation and simulation of its use, the MRS was exposed to temperatures
63 of up to 250°C, leading to significant oxidation of the CIPs and increase in the oxygen content
64 on their surfaces, rising from 0.47 wt% to 7 wt%. Indeed, a layer of iron oxide on the surfaces
65 of the CIPs also diminishes rheological parameters in the presence of a magnetic field (Plachy
66 et al. 2018, Ulicny, Balogh, Potter and Waldo 2007). Even though the MR effect of such a
67 device may only be slightly lessened in some cases (Roupec and Mazurek 2011), IUT
68 dramatically depreciates the properties of MRSs and raises operating demands connected to
69 lower performance and higher power consumption in the absence of a magnetic field, hence is
70 considered an undesirable phenomenon of MRSs (Carlson and Jolly 2000, Roupec and Mazurek
71 2011).

72 A potential means of improving the oxidation stability of the particles is to fabricate core-shell
73 particles, wherein the magnetic core is coated with a polymeric or inorganic shell (Cvek et al.
74 2015b, Han et al. 2018, Park et al. 2015, Park et al. 2016, Seo et al. 2018, Zhang et al. 2018).
75 Magnetorheological suspensions based on such composite particles have been shown to exhibit
76 a lower coefficient of friction compared to MRSs based on bare particles, as they can lower
77 their general abrasion and extend the service life of an MR device (Zhang, Dong, Choi and Lee
78 2018). Supplementing a non-magnetic polymeric layer on the surface of CIPs, however,
79 generally leads to decrease in values for saturation magnetization (M_s) (Lee et al. 2017,
80 Machovsky et al. 2014) of the particles; this plays an important role in determining the
81 rheological parameters of an MRS in the presence of a magnetic field. Cvek et al. (Cvek, Mrlik,
82 Ilcikova, Plachy, Sedlacik, Mosnacek and Pavlinek 2015b) have recently proposed surface-
83 initiated atom transfer radical polymerization (ATRP) as a tool to facilitate a controlled CIP
84 coating process. They demonstrated that the M_s of the core-shell CIPs (CIP-poly(glycidyl
85 methacrylate)) only decreased by about 4% in comparison with bare CIPs. An approach like
86 theirs could result in an MRS with heightened oxidation stability, wherein the M_s of the particles
87 is retained together with enhanced MR effects. Nevertheless, ATRP requires a complex reaction
88 system, usually one containing a copper halide catalyst and amide-based ligand (Matyjaszewski
89 2012). Removal of the catalyst is considered the main drawback, which alongside the air
90 sensitivity of the reaction, hinder general adoption by industry. These reasons explain the
91 motivation to introduce a different method capable of providing complementary results with
92 significant potential for practical application.

93 The goal of this study is to introduce a novel approach to coating a CIP surface with an organic
94 polymeric layer based on poly(amidoamine) (PAMAM) dendrons with step-by-step synthesis,
95 which enables control over the thickness of the layer. Poly(amidoamine) is a common
96 dendrimer that possesses a globular, monodisperse and highly branched structure (Fréchet J.M.J.
97 and D.A. 2001). It is prepared by sequential synthesis, facilitating the preparation of dendrimers
98 of various generations (G_x), permitting further definition of properties and size (Demir et al.
99 2014). For these reasons it represents a suitable candidate for application as an organic layer on
100 the surface of CIPs in magnetorheology, reducing the agglomeration of particles and
101 concurrently providing chemical and oxidation protection.

102 Herein, two novel magnetic core–shell particles were prepared, utilizing PAMAM dendrons of
103 generation 2 (G₂) and G_{2.5}. This led to formation of a very thin organic layer on the surface of
104 the CIPs, which preserved their level of M_s while also exhibiting enhanced thermal and
105 chemical stability. The MR performance of their MRSs was examined, and dynamic and static
106 yield stress values were estimated. Interestingly, the values for dynamic yield stress were found
107 to be ca 5% higher for the MRSs based on the coated particles than the reference MRS based
108 on carbonyl iron particles.

109 **Materials and methods**

110 *Materials and chemicals*

111 Commercial CIPs, grade SL ($d_{50} = 8.5 \mu\text{m}$; with a minimum Fe content of 99.5%) were obtained
112 from BASF (Germany). Ethylenediamine (ED; purity >99.5%), methyl acrylate (MA;
113 purity >99%) and potassium bromide (FT-IR grade, $\geq 99\%$ trace metals basis) were purchased
114 from Sigma-Aldrich (USA). The methyl acrylate and APTES were utilized in the form as
115 received, while the ED and anhydrous methanol were dried prior to use using layers of sodium
116 or molecular sieves, the latter at a mesh pore size of 0.3 nm. Hydrochloric acid (HCl), ethanol
117 (p.a.), acetone (p.a.) and toluene (purity >99%) were purchased from Penta Chemicals (Czech
118 Republic). Silicone oil (Lukosiol M200, Chemical Works Kolín, Czech Republic, viscosity
119 $\eta_c = 194 \text{ mPa s}$ at 25°C) was employed as a medium for preparing the MRSs.

120 *Application of CIP coating with PAMAM dendrons*

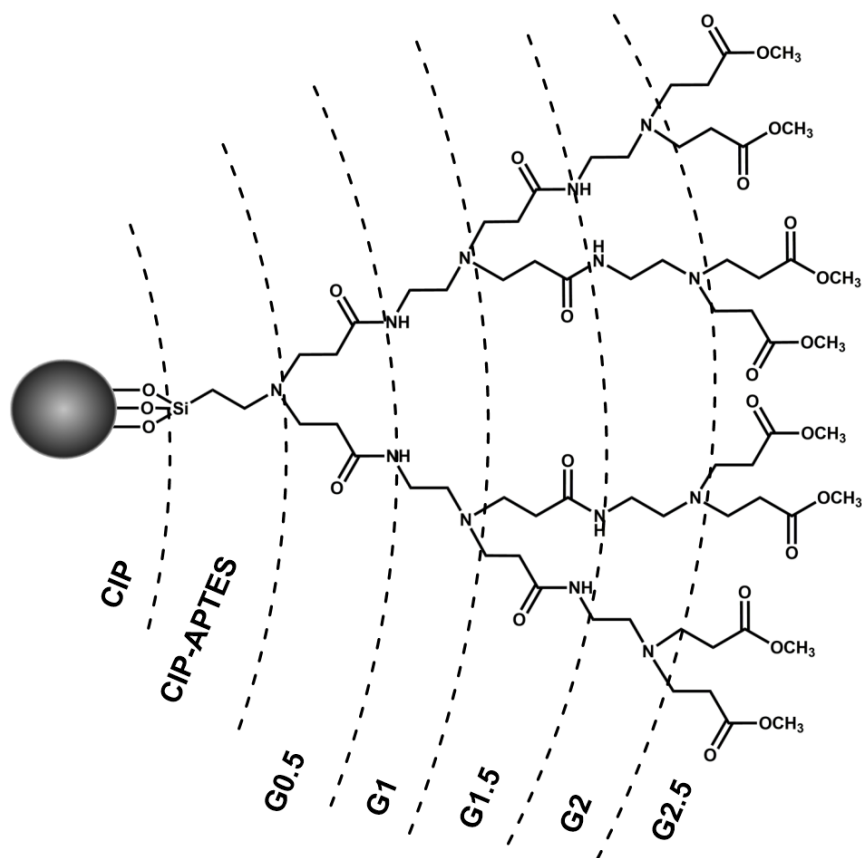
121 The surface of the CIPs was initially activated in order to create hydroxyl groups, besides
122 removing undesirable non-magnetic species from the surface, by 0.5 M HCl (Belyavskii et al.
123 2006). The particles were carefully washed afterwards in distilled water, ethanol and acetone.

124 A decantation process was carried out with a help of an external magnet; this occurring two
125 times with each of the above-mentioned liquids, and the mixture was mixed for approximately
126 10 minutes, followed by further drying at 60°C under the pressure of 200 mbar. These treated
127 particles were designated as CIP-0.

128 In the next step, the CIP-0 was modified with APTES to introduce $-NH_2$ groups onto their
129 surface (Belyavskii, Mingalyov, Giulieri, Combarrieau and Lisichkin 2006, Cvek, Mrlik,
130 Ilcikova, Plachy, Sedlacik, Mosnacek and Pavlinek 2015b) that could serve to facilitate the
131 growth of PAMAM dendrons. The CIP-0 particles (~44 g) were treated in a mixture of a
132 redundant amount of toluene (200 ml) and APTES (5 ml) at 110°C under vigorous stirring and
133 in a reflux system. After such treatment, the particles were rinsed and dried as previously. These
134 particles were designated as CIP-APTES.

135 The dendrons were grown in accordance with a synthesis procedure reported in the literature
136 (Fréchet J.M.J. and D.A. 2001). The dried CIP-APTES particles were mixed with anhydrous
137 methanol and MA was added drop-wise, where the amount of MA was in proportion to the
138 molar ratio 2:1 to the amount of APTES. The reaction took place in an N_2 atmosphere, under
139 vigorous stirring (250 rpm) and the fixed temperature of 5°C for the first hour. Subsequently,
140 the reaction proceeded for 24 hours at room temperature. The particles were washed after
141 treatment and dried as described previously. Following this, they were mixed with the
142 anhydrous methanol and ED was subsequently added drop-wise; the amount of ED was in
143 proportion to the molar ratio 1:1 to MA, as previously described. The reaction was performed
144 under an N_2 atmosphere and vigorous stirring (250 rpm), and maintained at 5°C for the first
145 hour. The reaction ran for 30 hours at room temperature, upon which the particles were rinsed
146 again and dried following the procedure given above.

147 The reaction of the particles with MA and ED was repeated several times, until particles of
148 generation GX had been prepared, where X represents the number of reactions with both MA
149 and ED (see Figure 1). Finally, the CIPs with PAMAM dendrons of G2 and G2.5 were obtained,
150 the particles of which being designated as CIP-PAMAM-G2 and CIP-PAMAM-G2.5,
151 respectively.



152

153 **Figure 1.** Schematic illustration of the hypothetical chemical composition and structure of the
 154 PAMAM dendron on the CIP.

155

156 *Particle characterization*

157 Sample imaging took place on a high resolution transmission electron microscope (HR-TEM)
 158 JEM 2100 (JEOL Japan), operated at the acceleration voltage of 180 kV, and equipped with a
 159 LaB6 cathode and a 5 megapixel TENGRA camera (Olympus, Germany). The diluted sample
 160 suspensions in methanol (5 mg/ml) were drop-cast onto carbon coated copper grids with a mesh
 161 size of 300 (Structure Probe Inc., USA) and dried at 70°C. The prepared particles were further
 162 characterized by diffuse reflectance infrared Fourier transform spectroscopy (DRIFT; Nicolet
 163 6700, Thermo Scientific, USA) in combination with KBr, Dispersive Raman microscopy
 164 (Nicolet DXR, Thermo Scientific, USA) and energy dispersive X-ray spectroscopy (EDXS)
 165 performed on an Octane SSD (area of 30 mm²) EDX detector (AMETEC) integrated into a
 166 scanning electron microscope (Nova NanoSEM 450, FEI company, Japan). Magnetic curves
 167 for the prepared samples were measured on a vibration sample magnetometer (VSM; Model
 168 7404, Lake Shore, USA) in the magnetic field range of $\pm 760 \text{ kA m}^{-1}$ at room temperature.
 169 Thermogravimetric analysis (TGA) was performed on a thermogravimetric analyser (TGA
 170 Q500, TA Instruments, USA) at a temperature range of 25–800°C in an N₂ atmosphere at a

171 heating rate of $10^{\circ}\text{C min}^{-1}$. X-ray photoelectron spectroscopy measurements were gauged on a
172 TFA XPS device (Physical Electronics). The base pressure in the XPS analysis chamber
173 equalled approximately 6×10^{-8} Pa. The samples were excited by X-rays over a $400 \mu\text{m}^2$ spot
174 area with monochromatic Al $K\alpha_{1,2}$ radiation at 1486.6 eV. Photoelectrons were detected by a
175 hemispherical analyser positioned at an angle of 45° from normal with respect to the sample
176 surface. Survey scan spectra were acquired at a pass energy of 187.85 eV and an energy step of
177 0.4 eV, whereas for Fe 2p, C 1s, O 1s, N 1s and Si 2p individual high-resolution spectra were
178 taken at the pass energy of 29.35 eV and energy step of 0.125 eV. All the spectra were
179 referenced to the main C 1s peak of the carbon atoms, which had been assigned a value of
180 284.8 eV. The spectra were analysed in MultiPak v8.1c software (Ulvac-Phi, Japan) from
181 Physical Electronics, which came supplied with the spectrometer.

182 *Preparation of magnetorheological suspensions and their characterization*

183 Magnetorheological suspensions containing 60 wt% of the particles were prepared by
184 dispersing the particles within the silicone oil. Thus, three different MR formulations containing
185 CIP-0, CIP-PAMAM-G2 and CIP-PAMAM-G2.5 particles were fabricated and labelled as
186 MRS-0, MRS-PAMAM-G2 and MRS-PAMAM-G2.5. Prior to each measurement, the
187 suspensions were thoroughly homogenized by mechanical mixing and ultrasonication (K-12LE,
188 Kraintek, Slovakia).

189 Magnetorheological measurements were performed on a rotational rheometer (MCR 502 Anton
190 Paar, Austria), with an external magnetic cell and gapped parallel plates of $300 \mu\text{m}$ (the width
191 between the upper and lower) in the presence of an external magnetic field of intensity 0–
192 438 kA/m at 25°C . MR characterization was conducted in shear test mode, involving both
193 controlled shear rate (CSR) and controlled shear stress (CSS). Measurement for the former was
194 performed at the shear rate of $0\text{--}80 \text{ s}^{-1}$; in the case of the latter, firstly measurements at the
195 constant shear rate of 50 s^{-1} were taken to obtain a value for shear stress, τ_{50} , and subsequently
196 a CSS ramp from 0 Pa to τ_{50} was applied.

197 Sedimentation stability was evaluated on a Krüss K100 Tensiometer (MK2/SF/C, Germany)
198 fitted with a SH0640 measuring probe, in the shape of an upside-down umbrella. The measuring
199 technique adopted was recently introduced, based on weight gain by the particles, which settled
200 into the probe immersed in the tested suspension after a certain period of time (Sedlacik and
201 Pavlinek 2014). Diluted MR suspensions containing 10 wt% of the particles were used for this
202 purpose.

203 Diluted MR suspensions supplemented with 20 wt% of the particles in silicone oil were
204 investigated by optical microscopy analysis. The samples were homogenized, then put between
205 two glass slides, and a magnetic field with magnetic flux density of 120 mT was applied to
206 create chain-like structures. The suspensions were observed on an optical microscope (Leica
207 DVM2500, Germany) linked to a digital camera.

208 **Results and discussion**

209 XPS analysis revealed that the CIP particles had been successfully coated with APTES, in
210 addition to further growth of the PAMAM dendrons (Li et al. 2016, Yin et al. 2015). While the
211 bare CIP particles only showed the presence of carbon, oxygen and iron, the CIP-APTES
212 particles possessed nitrogen and silicon from the APTES (Table 1). The carbon spectrum for
213 sample CIP-APTES was similar to that for the bare CIP sample (Figure 2a). In both cases, C–
214 C, C–OH and C=O groups were observed, however, the oxygen spectrum differed for the
215 sample with APTES (Figure 2b); two peaks were clearly visible - besides oxygen from the
216 oxidized iron, oxygen from the organic coating was evident. The CIP-APTES sample showed
217 a clear N 1s peak (Figure 3). The nitrogen peaks for CIP-PAMAM-G2 and CIP-PAMAM-G2.5
218 approximated the one for APTES (Figure 3). Since nitrogen is known for very slight chemical
219 shifts in binding energy, it is not possible to distinguish different configurations of nitrogen in
220 functional groups such as amino, amide or >N- , the presence of which would be expected
221 according to Figure 1.

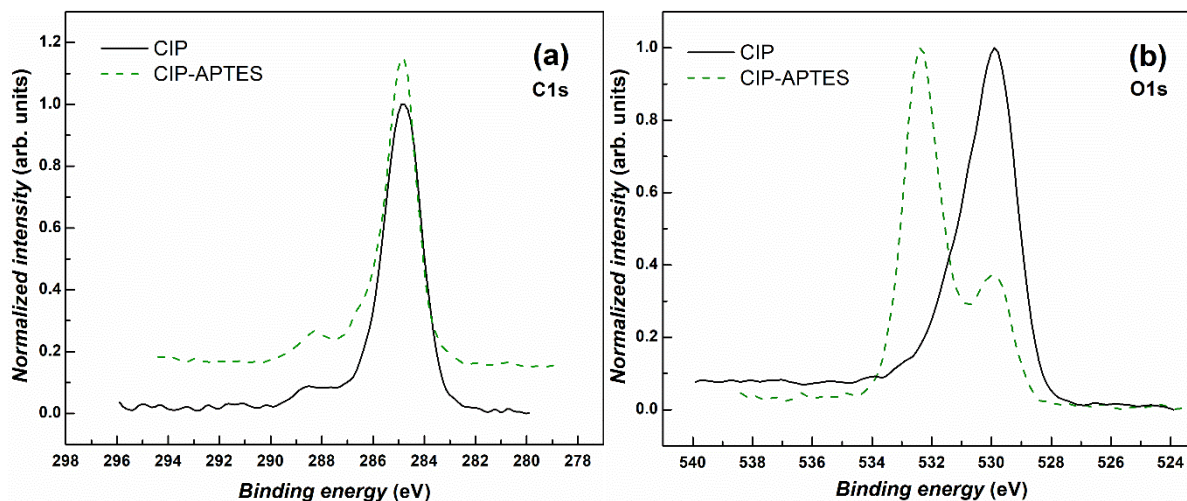
222

223

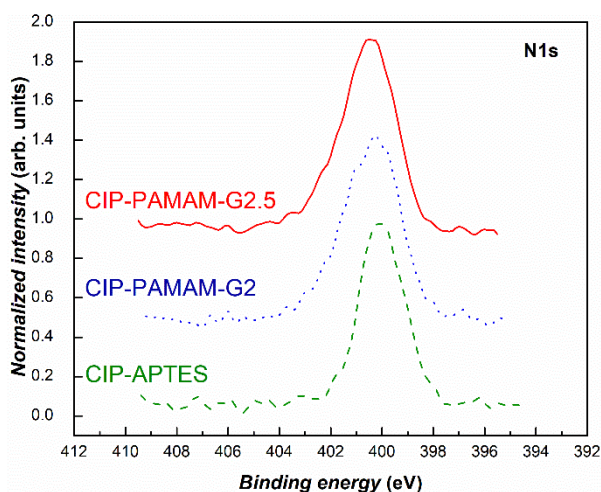
224 **Table 1.** Surface composition of the prepared samples in atomic per cent; the data were
225 obtained from XPS analysis.

| Sample | C | O | Fe | N | Si |
|-----------------------|----------|----------|-----------|----------|-----------|
| CIP | 31.9 | 52.7 | 15.4 | | |
| CIP-APTES | 46.3 | 31.0 | 3.4 | 6.6 | 12.8 |
| CIP-PAMAM-G2 | 49.2 | 30.8 | 3.0 | 10.5 | 6.4 |
| CIP-PAMAM-G2.5 | 49.7 | 31.0 | 3.0 | 8.8 | 7.5 |

226

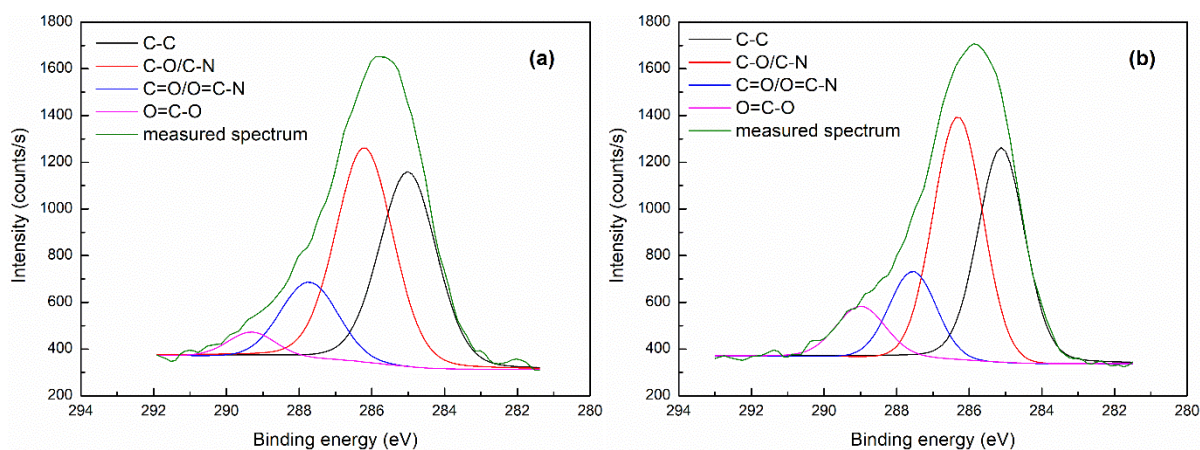


227
 228 **Figure 2.** Comparison of XPS high-resolution spectra for (a) C1s and (b) O1s of the CIP and
 229 CIP-APTES particles.



230
 231 **Figure 3.** XPS high-resolution spectra of N1s for the samples CIP-APTES, CIP-PAMAM-G2
 232 and CIP-PAMAM-G2.5.

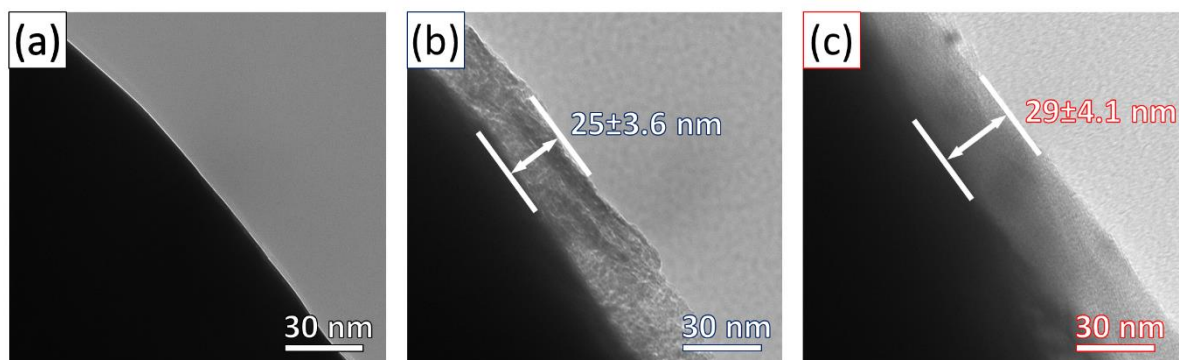
233
 234 Unlike nitrogen, the carbon spectra for CIP-PAMAM-G2, and CIP-PAMAM-G2.5 revealed
 235 significant differences from the carbon spectra for the CIP-APTES and CIP samples. The
 236 carbon spectra for the samples CIP-PAMAM-G2 and CIP-PAMAM-G2.5 were much wider
 237 than for CIP-APTES and CIP, indicating the presence of different functional groups originating
 238 from the PAMAM (Figure 4). Fitting the carbon spectra for the samples CIP-PAMAM-G2, and
 239 CIP-PAMAM-G2.5 showed some similarities, as functional groups such as C–OH/C–NH₂,
 240 C=O/N–C=O and O=C–OR were observed in both. Nevertheless, while the concentration of
 241 C–OH/C–NH₂ and C=O/N–C=O was almost the same, the concentration of O=C–OR was much
 242 higher for the sample CIP-PAMAM-G2.5 since acrylate constituted its top layer.



243
 244 **Figure 4.** Carbon C1s spectra with subcomponents for the samples (a) CIP-PAMAM-G2 and
 245 (b) CIP-PAMAM-G2.5

246
 247
 248
 249 Figure 5 shows TEM images of a bare particle and its modified analogues, demonstrating that
 250 the samples CIP-PAMAM-G2 and CIP-PAMAM-G2.5 clearly possessed a layer of coating on
 251 the surface of the particles. While CIP-0 had bare particles, a sharp contrast between the iron
 252 particle and background could be discerned. In the case of particles CIP-PAMAM-G2 and CIP-
 253 PAMAM-G2.5, a thin layer was distinguishable, confirming the formation of PAMAM
 254 dendrons on the surface of the CIP. The thickness (<30 nm) observed is highly desirable in the
 255 context of magnetorheology, since suppression of chemical and thermal oxidation of the
 256 particles is presumed to occur when values for M_s are maintained (Cvek et al. 2015a, Cvek,
 257 Mrlik, Ilcikova, Plachy, Sedlacik, Mosnacek and Pavlinek 2015b). It is worthy of note that the
 258 theoretical thickness of the layers, according to Figure 1, was significantly less than the
 259 thickness detected. It is known that during silanization of a surface with APTES, obtaining a
 260 monolayer of APTES is difficult to achieve. It is more likely that, under certain reaction
 261 conditions, a silane layer of ca 10 nm thick on the surface is possible (Aissaoui et al. 2012). A
 262 recognized aspect is that growth of a generation 2 PAMAM dendrimer can bring about rise in
 263 particle size by about 8 nm (Khodadust et al. 2013). In the case of dendron growth, some side
 264 reactions may occur due to the given concentrations of the monomers and reaction conditions;
 265 furthermore, due to polarization forces and adsorption, a dendrimer has the potential to increase
 266 the size of the particles to 15 nm (Baykal et al. 2012, Jafari-Soghieh et al. 2019). The thicker

267 layer discerned in this study could have been caused by either a trace amount of precursors
268 remaining on the particles after the washing cycle or the chosen precursor ratio.

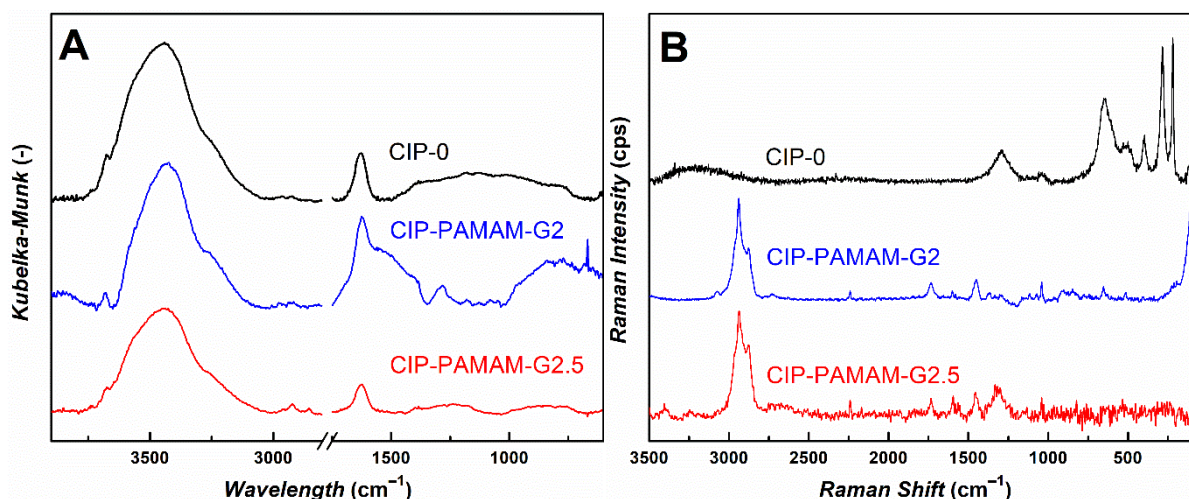


269
270 **Figure 5.** TEM images of (a) the bare CIP-0 and its analogues (b) CIP-PAMAM-G2 and (c)
271 CIP-PAMAM-G2.5.

272
273 The DRIFT spectra for the prepared samples showed a broad band in the region above 3200 cm^{-1}
274 $^{-1}$ and a medium band at 1628 cm^{-1} , ascribed to the moisture of the samples (Figure 6a). The
275 sample CIP-PAMAM-G2.5 also exhibited peaks at 2921 cm^{-1} and 2856 cm^{-1} typical for
276 PAMAM dendrons or dendrimers (Gautam S. P. et al. , Parsian et al. 2016), representing the
277 stretching of the functional groups $-\text{CH}_3$ and $-\text{CH}_2$, respectively. However, no other significant
278 peaks were presented due to very thin layer of PAMAM dendrons on the surface of the CIPs
279 (Figure 5).

280 Figure 6b details the Raman spectra for the bare CIP and PAMAM samples. These spectra are
281 not influenced by moisture, which significantly deteriorates infrared measurements and
282 associated bands that prevail in FTIR findings. Raman analysis clearly confirmed that the
283 PAMAM dendrons were present in both CIP-PAMAM samples. CIP-PAMAM-G2.5 contained
284 acrylate groups corresponding to bands at 1745 cm^{-1} and 1320 cm^{-1} , representing C=O and C-
285 O-C stretching, respectively; weak bands were also visible at 1040 cm^{-1} and 820 cm^{-1}
286 pertaining to skeletal vibrations of MA. The spectrum for CIP-PAMAM-G2 included bands at
287 1732 cm^{-1} and 1035 cm^{-1} , which probably constituted C=O stretching from the O=C-NH-C-
288 group and C-N stretching, respectively. The two spectra outlined above comprised similar
289 bands, however, interpretation of them was informed by the fact that G2 and G2.5 contained
290 acrylate and amine (amide) groups, respectively. The spectra for both CIP-PAMAM samples
291 featured bands in the regions $3000\text{--}2800\text{ cm}^{-1}$ and $1460\text{--}1455\text{ cm}^{-1}$, confirming the presence
292 of CH groups. Interestingly, the spectrum for Fe is typical for Fe_2O_3 , due to possible oxidation
293 of the surface layer of the particles, with no indication of acrylate and amine groups. This

294 confirmed that binding MA and ED to CIP-0 in step-wise synthesis had been successful and
 295 CIP-PAMAM particles had been created. It was not possible to carry out precise differentiation
 296 of the G2 and G2.5 dendrons any further with vibrational spectra, as certain Raman bands (e.g.
 297 C=O, N-C, N-H and others) were present in the Raman spectra and, thus, also in both CIP-
 298 PAMAM samples. This result corresponded to EDXS analysis, as described below.



299
 300 **Figure 6.** DRIFT (A) and Raman (B) spectra for the bare CIP-0 and its analogues CIP-
 301 PAMAM-G2 and CIP-PAMAM-G2.5.

302
 303 Table 2 lists the results of EDXS, a semi-quantitative analysis describing the chemical
 304 composition of a surface of a material (from depth upwards, in units of μm). Besides iron, the
 305 CIP-0 sample contained a small amount of carbon and oxygen, the former originating from iron
 306 pentacarbonyl - a precursor for preparing CIPs, while the latter comes from the hydroxyl groups
 307 on the surface of the particles; however, it is not possible to fully disprove the presence of iron
 308 oxide. As for CIP-PAMAM-G2 and CIP-PAMAM-G2.5, the small portions of nitrogen and
 309 silicon from the APTES and PAMAM dendrons confirmed that the coating process of the CIP-
 310 0 with PAMAM dendrons had taken place successfully.

311
 312
 313
 314 **Table 2.** Results of EDXS analysis (values are given in weight per cent) and the saturation
 315 magnetization values for the prepared particles.

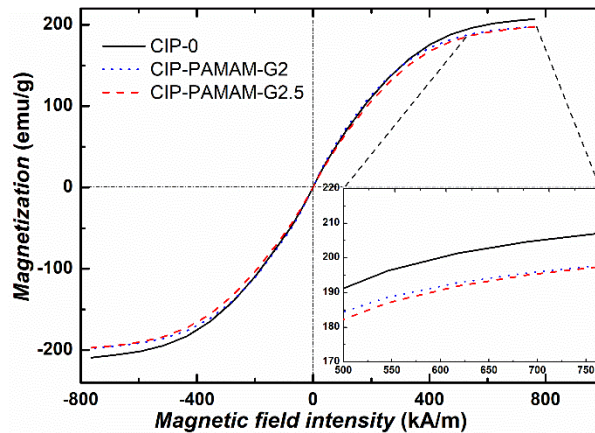
| Element | CIP-0 (wt%) | CIP-PAMAM-G2 (wt%) | CIP-PAMAM-G2.5 (wt%) |
|---------|-----------------|--------------------|----------------------|
| C | 3.06 ± 0.18 | 2.88 ± 0.19 | 3.37 ± 0.20 |

| | | | |
|---|------------------|------------------|------------------|
| N | – | 0.38 ± 0.17 | 0.43 ± 0.19 |
| O | 1.28 ± 0.09 | 1.14 ± 0.10 | 1.13 ± 0.11 |
| Si | – | 0.15 ± 0.03 | 0.13 ± 0.03 |
| Fe | 95.66 ± 0.20 | 95.18 ± 0.26 | 94.94 ± 0.29 |
| <hr/> | | | |
| <i>Magnetic saturation</i> | | | |
| <i>M_S (emu/g)</i> | 207.0 | 197.7 | 197.3 |
| <i>Decrease in M_S</i> | | | |
| <i>against CIP-0 (%)</i> | - | 4.5 | 4.7 |

316

317

318 The value for M_S of the magnetic particles is important in relation to the MR effect of an MRS.
 319 In low magnetic fields, yield stress (τ_y) - the minimal amount of stress that has to be applied
 320 before the system starts to flow - is primarily dependent on magnetic field intensity, scaling as
 321 $\tau_y \sim H^2$; with increase in the intensity of the magnetic field, M_S emerges as an important
 322 parameter, and τ_y scales as $\tau_y \sim M_S^{1/2} H^{3/2}$ (Fang et al. 2011, Ginder et al. 1996). It is consequently
 323 crucial to follow a controlled procedure for coating magnetic particles in order to keep values
 324 for M_S as high as possible. Herein, the CIP coating process only subtly affected the M_S values
 325 for the prepared particles (Figure 7), which is a desirable quality for an MRS since its MR effect
 326 persists correspondingly. The M_S values for the samples are given in Table 2, revealing that the
 327 M_S for the sample with the greatest dendron generation of a non-magnetic layer on its surface
 328 (CIP-PAMAM-G2.5) merely decreased by about 4.7% compared to the neat CIPs (CIP-0). This
 329 finding is similar to the lowest drop in M_S values found in the literature, wherein atom transfer
 330 radical polymerization was employed for controlled application of layers of a polymeric coating
 331 on CIPs (Cvek, Mrlik, Ilcikova, Plachy, Sedlacik, Mosnacek and Pavlinek 2015b).

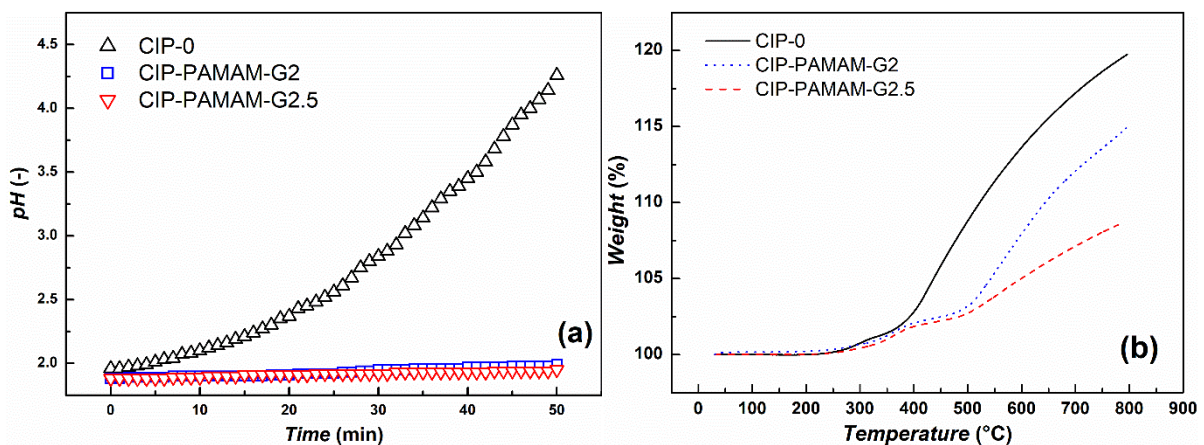


332

333 **Figure 7.** Magnetic curves for the bare CIP-0 and its analogues CIP-PAMAM-G2 and CIP-
 334 PAMAM-G2.5.

335

336 Oxidation stability in an acidic solution is a test often performed to gauge improvement in
 337 chemical stability and confirm the presence of a compact coating on particles. Rise in pH value
 338 during the treatment of CIP-0 in 0.05 M solution of HCl (Figure 8a) indicated that oxidation of
 339 the particles had occurred, evident through neutralization of the acidic solution. In contrast, CI-
 340 PAMAM-G2 and CI-PAMAM-G2.5, with a thin layer of coating on their respective surfaces,
 341 showed high stability in acidic conditions, confirming the PAMAM coating was free of defects
 342 and able to inhibit contact between the acidic solution and the iron core. This extreme stability
 343 suggests that the uniform coating in place could additionally protect the iron particles from
 344 entry by moisture or other substances containing oxygen during use, thus preventing oxidation
 345 from affecting the service life of any instruments featuring them. Figure 8b depicts the change
 346 in weight exhibited by the prepared particles during heat treatment in a N₂ atmosphere at up to
 347 800°C. In the case of CIP-0, the particles were stable until 370°C, whereupon an abrupt gain in
 348 weight by the particles occurred. Even though the test happened in a N₂ atmosphere, the weight
 349 of the samples increased considerably during the heating process. The gain in weight could
 350 been arisen from initiation of a nitriding phase, causing formation of Fe₄N or various Fe₃N_x
 351 (Konig et al. 2017). Nevertheless, the particles still possessed omnipresent oxygen adsorbed to
 352 their surfaces with the potential to oxidise them. The coated particles demonstrated improved
 353 thermal stability upon a sudden increase in weight at 500°C. It has been stated in the literature
 354 that - concurrent with or following thermal decomposition of a polymeric layer - should a
 355 nitriding phase develop or the particles oxidise, thermal decomposition of the polymer still takes
 356 place, despite the fact that no decrease in weight is evident (Cvek, Mrlik, Ilcikova, Plachy,
 357 Sedlacik, Mosnacek and Pavlinek 2015b).



358

359 **Figure 8.** (a) Oxidation stability of the bare CIP-0 and its analogues CIP-PAMAM-G2 and CIP-
 360 PAMAM-G2.5, as tested in 0.05 M solution of HCl at room temperature in relation to the
 361 dependence of pH values of the solution over time. (b) TGA curves for the bare CIP-0 and its

362 analogues CIP-PAMAM-G2 and CIP-PAMAM-G2.5, as tested in an N₂ atmosphere at a heating
363 rate of 10°C min⁻¹.

364

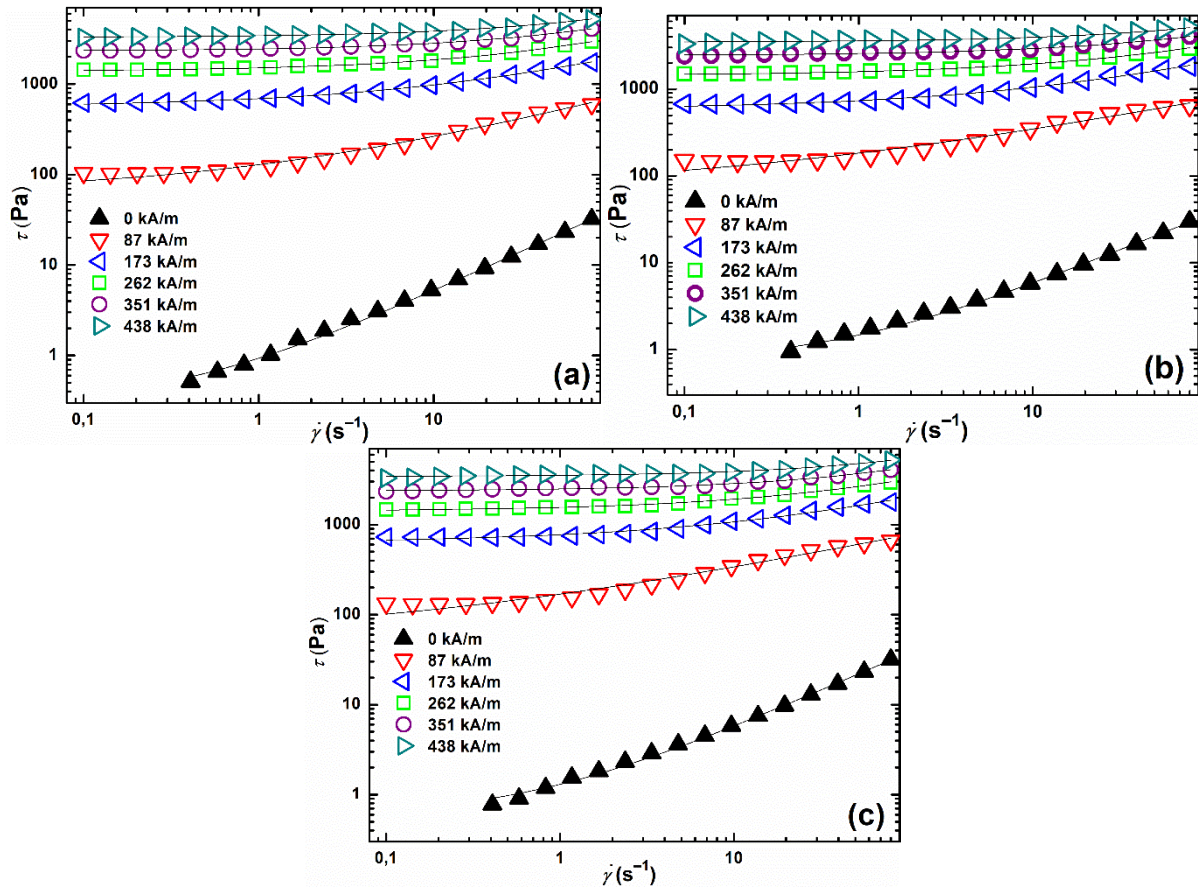
365 *Magnetorheology and sedimentation stability*

366 The MRSs exhibited transition from liquid to a solid-like state after applying an external
367 magnetic field, a typical characteristic for an MRS. In the absence of an external magnetic field
368 they demonstrated slightly pseudoplastic behaviour, whereas in a presence of one their values
369 for shear stress increased by several orders of magnitude and they exhibited field-dependent
370 values for τ_y (Figure 9) (Anupama et al. 2019, Kwon et al. 2020). Several rheological models
371 are capable of estimating τ_y for an MRS. Even though some exist with the capability to fit flow
372 curves (Cvek et al. 2016, Seo, Han, Choi, Takahara, Choi and Seo 2018), for reasons of
373 feasibility and simplicity, herein the classic Herschel-Bulkley (H-B) rheological model was
374 employed to fit the experimental data. The H-B equation is expressed below (Equation 1),
375 where K represents the consistency index and n is the non-Newtonian flow index.

$$376 \quad \tau = K \cdot \dot{\gamma}^n + \tau_y \quad (1)$$

377 The field-off viscosities of the MRSs based on coated particles have the potential to slightly
378 exceed the value for MRS-CIP, since the branched polymeric surfaces on CI-PAMAM-G2 and
379 CI-PAMAM-G2.5 increase interactions between both them and the carrier fluid (silicone oil),
380 which brings about a minor decrease in the parameter n from 0.89 to 0.84 that describes the
381 evolved pseudoplasticity of the system (Table 3). Interestingly, values for τ_y are higher for the
382 MRSs based on coated particles than MRS-CIP (Table 3). The polymeric coating should hinder
383 possible particle agglomeration and improve the arrangement of particles upon application of a
384 magnetic field, thereby enhancing the MR effect of the MRS (Lopez-Lopez et al. 2008b). When
385 tested with the strongest applied magnetic field of 438 kA m⁻¹, the MRSs with coated particles
386 (CI-PAMAM-G2 and CI-PAMAM-G2.5) exhibited τ_y values approximately 4.8% and 4.0%
387 higher than the reference MRS, respectively. Thus, the ability to control the thickness of the
388 organic layer on magnetic particles in an MRS could result in suitable particles with
389 significantly heightened oxidation stability as well as the absence of any undesirable decrease
390 in MR performance by the MRS.

391



392

393

394 **Figure 9.** Log-log dependencies of shear stress on the shear rate for the prepared MRSs: (a)
 395 MRS-CIP, (b) MRS-PAMAM-G2 and (c) MRS-PAMAM-G2.5 in various magnetic fields;
 396 measurements were performed in CSR mode, and the solid lines represent the H-B fit.

397

398

399

400

401

402

403

404

405

406

407

408

409

410 **Table 3.** Values for rheological parameters obtained from the H-B model and τ_{stat} values for the
 411 prepared MRSs at various intensities of magnetic field.

| Sample | Parameter | Magnetic field intensity (kA/m) | | | | | |
|----------------------------|---------------------------|---------------------------------|------|------|-------|-------|-------|
| | | 0 | 87 | 173 | 262 | 351 | 438 |
| MRS-CIP | n [-] | 0.89 | 0.50 | 0.51 | 0.58 | 0.60 | 0.61 |
| | K [Pa s ⁿ] | 0.64 | 63 | 128 | 121 | 127 | 137 |
| | τ_y [Pa] | 0.29 | 65 | 563 | 1 390 | 2 320 | 3 290 |
| MRS-PAMAM-G2 | n [-] | 0.85 | 0.31 | 0.45 | 0.54 | 0.59 | 0.64 |
| | K [Pa s ⁿ] | 0.76 | 113 | 147 | 147 | 130 | 124 |
| | τ_y [Pa] | 0.71 | 70 | 597 | 1 440 | 2 430 | 3 450 |
| MRS-PAMAM-G2.5 | n [-] | 0.85 | 0.40 | 0.49 | 0.55 | 0.60 | 0.64 |
| | K [Pa s ⁿ] | 0.73 | 112 | 144 | 144 | 124 | 110 |
| | τ_y [Pa] | 0.57 | 57 | 629 | 1 410 | 2 370 | 3 420 |
| Static yield stress values | Parameter | Magnetic field intensity (kA/m) | | | | | |
| | | 0* | 87 | 173 | 262 | 351 | 438 |
| MRS-CIP | τ_{stat} [Pa] | – | 239 | 961 | 1870 | 2920 | 4140 |
| MRS-PAMAM-G2 | τ_{stat} [Pa] | – | 261 | 817 | 1880 | 2960 | 4000 |
| MRS-PAMAM-G2.5 | τ_{stat} [Pa] | – | 219 | 910 | 1760 | 2850 | 3930 |

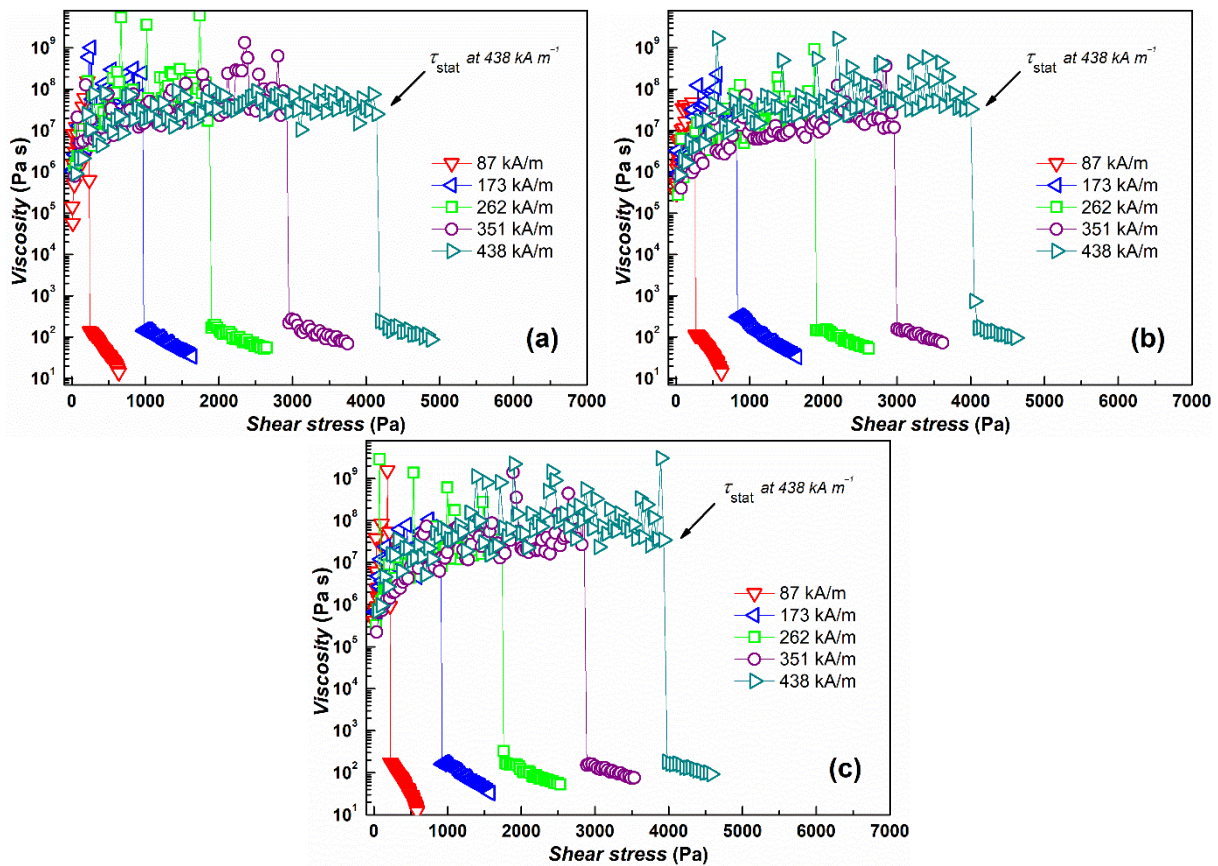
412 *The prepared MRSs did not exhibit any inherent τ_{stat} .

413

414 Another way to evaluate the stiffness of an MRS is to determine static yield stress, denoted
 415 as τ_{stat} , and different methods exist to do so experimentally (De Vicente et al. 2010, Yang et al.
 416 2009). Controlled shear stress measurement, with an ascending shear stress ramp rising to the
 417 value τ_{50} , was employed for this purpose. In this context, no macroscopic flow occurs in the
 418 system below τ_{stat} , as represented by high values for viscosity. When the value for shear stress
 419 exceeds that for τ_{stat} , flow is initiated and an abrupt drop in viscosity is observed (Figure 10).
 420 The final value recorded for shear stress before such dramatic reduction in viscosity is
 421 designated as τ_{stat} (De Vicente, Vereda, Segovia-Gutierrez, Morales and Hidalgo-Alvarez 2010,
 422 Fang, Liu, Choi and Seo 2011). In tests, unlike the τ_y values, τ_{stat} was found to be higher for
 423 MRS-CIP than systems with coated particles, even though the difference is less than <6% at
 424 the magnetic field intensity of 438 kA m⁻¹ (Table 3). It should be further noted that τ_{stat} values
 425 were generally higher than τ_0 values due to the different origins of both phenomena and methods

426 for their estimation. While τ_y is estimated by indirect methods (De Vicente, Klingenberg and
 427 Hidalgo-Alvarez 2011), τ_{stat} , which is often referred to as frictional yield stress, is considered
 428 collapse of the top layer of a built-up structure close to the moving part of its geometry (or
 429 “slip”), rather than the collapse of built-up structures throughout the MRS (Volkova et al. 2000).
 430 Having a coating on the particles can prevent them from agglomerating and facilitate enhanced
 431 arrangement of them upon application of a magnetic field as a consequence; in addition, they
 432 demonstrate higher τ_y values than bare CIPs (Lopez-Lopez, Zugaldia, Gomez-Ramirez,
 433 Gonzalez-Caballero and Duran 2008b). In the case of τ_{stat} , its values are not significantly
 434 affected by such built-up structures, since particles collapse from the top part of the measured
 435 geometry.

436



438

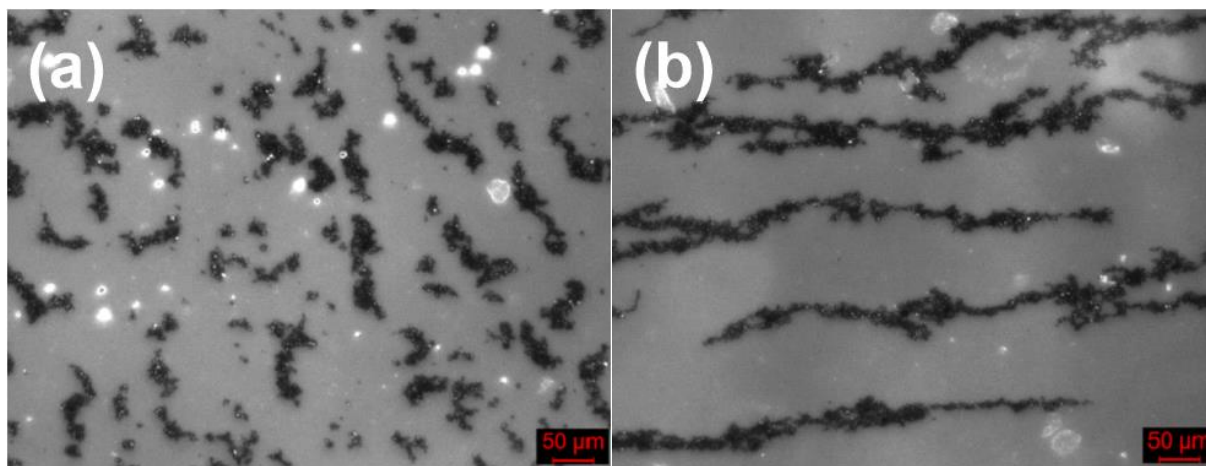
439

440 **Figure 10.** Dependencies of viscosity on shear stress for the prepared MRSs: (a) MRS-CIP, (b)
 441 MRS-PAMAM-G2 and (c) MRS-PAMAM-G2.5 in various magnetic fields; measurements
 442 were performed in CSS mode.

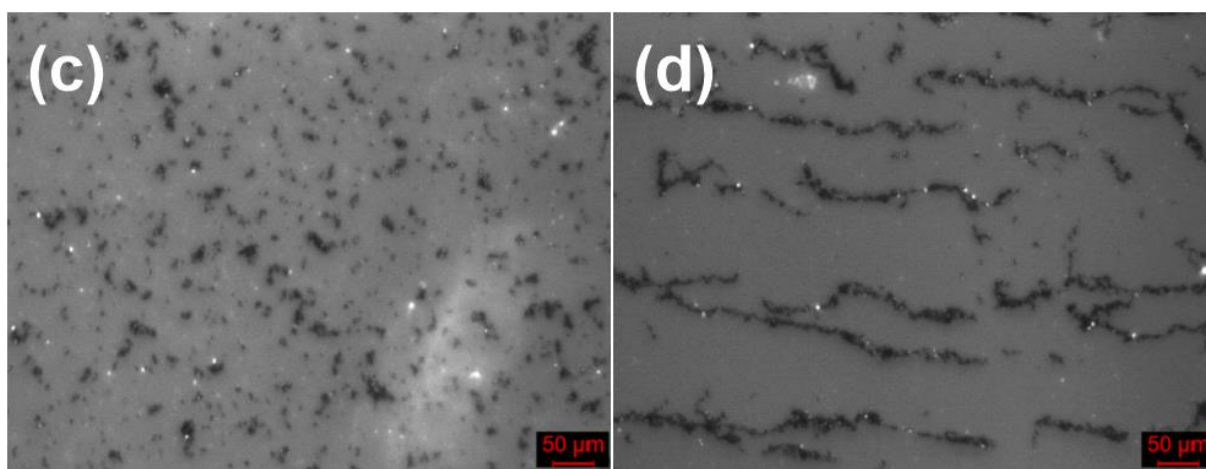
443

444 The fact that CIP formed agglomerates in the silicone oil is evident from images obtained from
445 optical microscopy (Figure 11a). Since such particles possess a polar surface, they tend to group
446 together in silicone oil. The coated surfaces of those in CIP-PAMAM-G2 and CIP-PAMAM-
447 G2.5 led to good dispersion in the liquid medium, both exhibiting a low amount of agglomerates
448 of small size compared to CIPs (Figure 11c, e). After applying a magnetic field, the particles
449 created chain-like structures in the direction of the magnetic field (Figure 11b, d, f). While thick
450 CIP chains of agglomerates were evident, CIP-PAMAM-G2 and CIP-PAMAM-G2.5 created
451 thinner columns of coated particles that were more uniform than the CIP chains. Comparing
452 CIP-PAMAM-G2 and CIP-PAMAM-G2.5 with a terminating $-NH_2$ group or $-O-CH_3$, the
453 former demonstrated less aggregation than the latter.

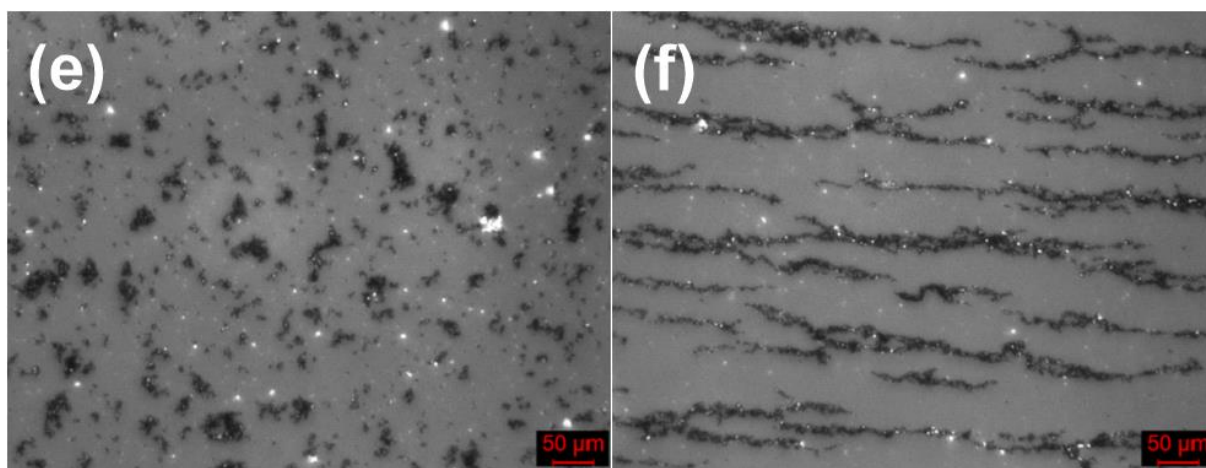
454



455



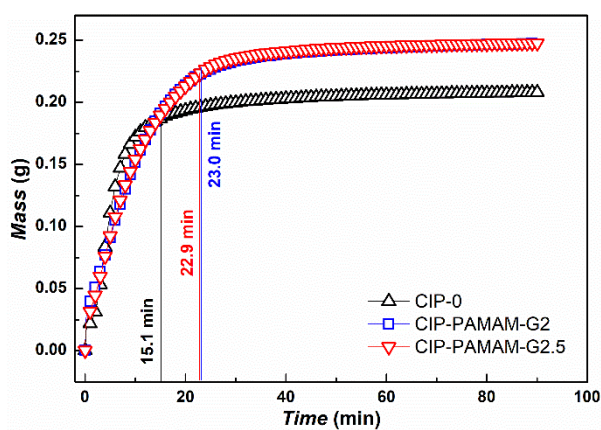
456



457 **Figure 11.** Optical microscopy of a 20 wt% silicone oil suspensions of (a, b) CIP-0, (c, d) CI-
 458 PAMAM-G2 and (e,f) CI-PAMAM-G2.5). Images (a), (c) and (e) are taken in the absence of a
 459 magnetic field; images (b), (d) and (f) are taken in the presence of a magnetic field with
 460 magnetic flux density of 120 mT.

461 Poor sedimentation stability is another drawback of MRSs that has to be overcome for possible
 462 everyday applications. Although the coating process of the particles itself does not provide
 463 MRSs with long-term stability, it can reduce the sedimentation rate of the particles, which takes

464 place through decrease in overall density of the particles and heightened friction forces between
465 the particles and carrier fluid. Furthermore, coating the particles also diminishes their tendency
466 to agglomerate, potentially lending the system greater stability (Lopez-Lopez et al. 2008a).
467 Figure 12 details measurements of sedimentation stability for the prepared MRSs. These
468 describe a comparative approach for the given MRSs and are expressed as t_{90} , i.e. the time in
469 which 90% of the particles from the area above the probe settle into it. While t_{90} was 15.1 min
470 for MRS-CIP, the same for the two MRSs based on the PAMAM coated particles were found
471 to be ~ 23.0 min. for both. Unfortunately, it is not possible to compare the findings with another
472 MRS due to unique nature of the sedimentation testing method adopted.



473
474 **Figure 12.** Test of sedimentation stability of the prepared MRSs; results are expressed as the
475 mass of particles settled in the measuring probe over a certain period of time.

476 Conclusions

477 This paper presents application of a coating of carbonyl iron particles with poly(amidoamine)
478 dendrons as an efficient means for preventing particle oxidation and extending the service life
479 of suspensions. The particles were coated with poly(amidoamine) of 2 and 2.5 generations,
480 giving rise to different functional groups on their surfaces. The thickness of the dendritic layers
481 equalled approximately 30 nm, which provided sufficient thermal and chemical oxidation
482 stability, as tested by thermogravimetric analysis and treatment in an acidic solution, thereby
483 confirming the particles had been completely coated. In addition, their saturation magnetization
484 decreased by only ca 4.5% compared to the bare carbonyl iron particles. The particles were
485 further employed as a dispersed phase in magnetorheological suspensions, and their
486 performance was investigated through measuring controlled shear rate and controlled shear
487 stress in order to determine dynamic yield stress, conducted by means of the Herschel-Bulkley

488 model and static yield stress. Interestingly, the magnetorheological suspensions based on coated
489 particles exhibited values of ca 4% higher for dynamic yield stress, as well as demonstrating
490 enhanced sedimentation stability, compared to magnetorheological suspensions based on the
491 original carbonyl iron particles. Optical microscopy revealed that the organic layer on the
492 surface hinders the coated particles from forming agglomerates; thus, as stated in the literature,
493 the potential exists for developing MR suspensions with heightened magnetorheological effects.
494 Such coated particles would appear to make it possible to prepare magnetorheological
495 suspensions with high oxidation stability, thereby overcoming the issue of in-use-thickening
496 which is known to limit the utilization of magnetorheological suspensions, with the consequent
497 advantage of persistent high performance in the presence of a magnetic field. In addition, the
498 improvement in reduced abrasion of the particles during their use can be expected.

499

500 **Author information**

501 *Corresponding Author*

502 *E-mail: plachy@utb.cz

503

504 *Notes*

505 The authors declare no competing financial interests.

506 *Conflicts of interest*

507 There are no conflicts to declare.

508 *Data availability*

509 The datasets generated and/or analysed during the current study are available from the corresponding
510 author upon request.

511

512 **Acknowledgements**

513 This work was supported by the Ministry of Education, Youth and Sports of the Czech Republic
514 – DKRVO (RP/CPS/2020/003) and DKRVO (RP/CPS/2020/006). Research was also aided by
515 the Operational Programme Research and Development for Innovations initiative co-funded by
516 the European Regional Development Fund (ERDF) and the state budget of the Czech Republic,
517 within the framework of a Centre of Polymer Systems project (CZ.1.05/2.1.00/19.0409).

518

519 **References**

520

- 522 Aissaoui N, Bergaoui L, Landoulsi J, Lambert JF, Boujday S (2012) Silane Layers on Silicon Surfaces:
523 Mechanism of Interaction, Stability, and Influence on Protein Adsorption. *Langmuir* 28: 656-
524 665. <https://doi.org/10.1021/la2036778>
- 525 Anupama AV, Kumaran V, Sahoo B (2019) Synthesis of highly magnetic Mn-Zn ferrite
526 (Mn_{0.7}Zn_{0.3}Fe₂O₄) ceramic powder and its use in smart magnetorheological fluid. *Rheol Acta*
527 58: 273-280. <https://doi.org/10.1007/s00397-019-01137-z>
- 528 Baykal A, Toprak MS, Durmus Z, Senel M, Sozeri H, Demir A (2012) Synthesis and Characterization of
529 Dendrimer-Encapsulated Iron and Iron-Oxide Nanoparticles. *J Supercond Nov Magn* 25: 1541-
530 1549. <https://doi.org/10.1007/s10948-012-1454-z>
- 531 Bell RC, Karli JO, Vavreck AN, Zimmerman DT, Ngatu GT, Wereley NM (2008) Magnetorheology of
532 submicron diameter iron microwires dispersed in silicone oil. *Smart Mater Struct* 17: 6.
533 <https://doi.org/10.1088/0964-1726/17/01/015028>
- 534 Belyavskii SG, Mingalyov PG, Giulieri F, Combarrieau R, Lisichkin GV (2006) Chemical modification of
535 the surface of a carbonyl iron powder. *Protect Met* 42: 244-252.
536 <https://doi.org/10.1134/s0033173206030064>
- 537 Bombard AJF, Goncalves FR, de Vicente J (2015) Magnetorheology of Carbonyl Iron Dispersions in 1-
538 Alkyl-3methylimidazolium Ionic Liquids. *Ind Eng Chem Res* 54: 9956-9963.
539 <https://doi.org/10.1021/acs.iecr.5b02824>
- 540 Bucchi F, Forte P, Franceschini A, Frendo F (2013) Analysis of differently sized prototypes of an MR
541 clutch by performance indices. *Smart Materials and Structures* 22: 10.
542 <https://doi.org/10.1088/0964-1726/22/10/105009>
- 543 Carlson JD, Jolly MR (2000) MR fluid, foam and elastomer devices. *Mechatronics* 10: 555-569.
544 [https://doi.org/10.1016/s0957-4158\(99\)00064-1](https://doi.org/10.1016/s0957-4158(99)00064-1)
- 545 Cvek M, Mrlik M, Ilcikova M, Mosnacek J, Babayan V, Kucekova Z, Humpolicek P, Pavlinek V (2015a)
546 The chemical stability and cytotoxicity of carbonyl iron particles grafted with poly(glycidyl
547 methacrylate) and the magnetorheological activity of their suspensions. *RSC Adv* 5: 72816-
548 72824. <https://doi.org/10.1039/c5ra11968e>
- 549 Cvek M, Mrlik M, Ilcikova M, Plachy T, Sedlacik M, Mosnacek J, Pavlinek V (2015b) A facile controllable
550 coating of carbonyl iron particles with poly(glycidyl methacrylate): a tool for adjusting MR
551 response and stability properties. *J Mater Chem C* 3: 4646-4656.
552 <https://doi.org/10.1039/c5tc00319a>
- 553 Cvek M, Mrlik M, Pavlinek V (2016) A rheological evaluation of steady shear magnetorheological flow
554 behavior using three-parameter viscoplastic models. *J Rheol* 60: 687. <https://doi.org/10.1122/1.4954249>
- 556 Cvek M, Torres-Mendieta R, Havelka O, Urbanek M, Plachy T, Cernik M (2020) Laser-induced
557 fragmentation of carbonyl iron as a clean method to enhance magnetorheological effect. *J*
558 *Clean Prod* 254: 8. <https://doi.org/10.1016/j.jclepro.2020.120182>
- 559 de Vicente J, Klingenberg DJ, Hidalgo-Alvarez R (2011) Magnetorheological fluids: a review. *Soft Matter*
560 7: 3701-3710. <https://doi.org/10.1039/c0sm01221a>
- 561 de Vicente J, Vereda F, Segovia-Gutierrez JP, Morales MD, Hidalgo-Alvarez R (2010) Effect of particle
562 shape in magnetorheology. *J Rheol* 54: 1337-1362. <https://doi.org/10.1122/1.3479045>
- 563 Demir M, Senel M, Baykal A (2014) Reversible immobilization of BSA on Cu-chelated PAMAM
564 dendrimer modified iron oxide nanoparticles. *Appl Surf Sci* 314: 697-703.
565 <https://doi.org/10.1016/j.apsusc.2014.07.082>
- 566 Fang FF, Liu YD, Choi HJ, Seo Y (2011) Core-Shell Structured Carbonyl Iron Microspheres Prepared via
567 Dual-Step Functionality Coatings and Their Magnetorheological Response. *ACS Appl Mater*
568 *Interfaces* 3: 3487-3495. <https://doi.org/10.1021/am200714p>
- 569 Feijoo AV, Lopez-Lopez MT, Galindo-Gonzalez C, Stange S, Nguyen TT, Mammeri F, Merah S, Ponton A
570 (2020) Rheological investigation of magnetic sensitive biopolymer composites: effect of the

571 ligand grafting of magnetic nanoparticles. *Rheol Acta* 59: 165-176.
572 <https://doi.org/10.1007/s00397-020-01191-y>

573 Fréchet J.M.J., D.A. T (2001) *Dendrimers and Other Dendritic Polymers*. John Wiley & Sons, Edithvale
574 (Australia)

575 Gautam S. P., Keservani R. K., Gautam T., Gupta A. K., K. SA An Alternative Approach for Acetylation of
576 Amine Terminated Polyamidoamine (PAMAM) Dendrimer. *Ars Pharmaceutica* 56: 155-159.

577 Ginder JM, Davis LC, Elie LD (1996) Rheology of magnetorheological fluids: Models and measurements.
578 *Int J Mod Phys B* 10: 3293-3303. <https://doi.org/10.1142/s0217979296001744>

579 Han JK, Lee JY, Choi HJ (2019) Rheological effect of Zn-doped ferrite nanoparticle additive with
580 enhanced magnetism on micro-spherical carbonyl iron based magnetorheological suspension.
581 *Colloid Surf A-Physicochem Eng Asp* 571: 168-173.
582 <https://doi.org/10.1016/j.colsurfa.2019.03.084>

583 Han S, Choi J, Seo YP, Park IJ, Choi HJ, Seo Y (2018) High-performance magnetorheological suspensions
584 of pickering-emulsion-polymerized polystyrene/Fe₃O₄ particles with enhanced stability.
585 *Langmuir* 34: 2807-2814. <https://doi.org/10.1021/acs.langmuir.7b04043>

586 Chen ZQ, Wang XY, Ko JM, Ni YQ, Spencer BF, Yang G (2003) MR damping system on Dongting Lake
587 cable-stayed bridge. In: Liu SC (ed) *Smart Structures and Materials 2003: Smart Systems and*
588 *Nondestructive Evaluation for Civil Infrastructures*, vol 5057. Spie-Int Soc Optical Engineering,
589 Bellingham, pp 229-235

590 Jafari-Soghieh F, Maleki B, Behniafar H (2019) Effect of dendrimer-functionalized magnetic iron oxide
591 nanoparticles on improving thermal and mechanical properties of DGEBA/IPD epoxy networks.
592 *High Performance Polymers* 31: 24-31. <https://doi.org/10.1177/0954008317749020>

593 Khodadust R, Unsoy G, Yalcin S, Gunduz G, Gunduz U (2013) PAMAM dendrimer-coated iron oxide
594 nanoparticles: synthesis and characterization of different generations. *J Nanopart Res* 15: 13.
595 <https://doi.org/10.1007/s11051-013-1488-6>

596 Konig R, Muller S, Dinnebier RE, Hinrichsen B, Muller P, Ribbens A, Hwang J, Liebscher R, Etter M,
597 Pistidda C (2017) The crystal structures of carbonyl iron powder - revised using in situ
598 synchrotron XRPD. *Z Krist-Cryst Mater* 232: 835-842. <https://doi.org/10.1515/zkri-2017-2067>

599 Kwon SH, Hong CH, Do PX, Choi SB, Choi HJ (2015) Magnetorheology of a carbonyliron microsphere
600 suspension with a halloysite additive and its damping force characteristics. *Ind Eng Chem Res*
601 54: 4655-4663. <https://doi.org/10.1021/acs.iecr.5b00233>

602 Kwon SH, Na SM, Flatau AB, Choi HJ (2020) Fe-Ga alloy based magnetorheological fluid and its
603 viscoelastic characteristics. *J Ind Eng Chem* 82: 433-438.
604 <https://doi.org/10.1016/j.jiec.2019.11.007>

605 Lee JW, Hong KP, Kwon SH, Choi HJ, Cho MW (2017) Suspension rheology and magnetorheological
606 finishing characteristics of biopolymer-coated carbonyliron particles. *Ind Eng Chem Res* 56:
607 2416-2424. <https://doi.org/10.1021/acs.iecr.6b03790>

608 Li YZ, Guan YQ, Liu Y, Yin JB, Zhao XP (2016) Highly stable nanofluid based on polyhedral oligomeric
609 silsesquioxane-decorated graphene oxide nanosheets and its enhanced electro-responsive
610 behavior. *Nanotechnology* 27: 11. <https://doi.org/10.1088/0957-4484/27/19/195702>

611 Lopez-Lopez MT, Kuzhir P, Bossis G, Mingalyov P (2008a) Preparation of well-dispersed
612 magnetorheological fluids and effect of dispersion on their magnetorheological properties.
613 *Rheol Acta* 47: 787-796. <https://doi.org/10.1007/s00397-008-0271-6>

614 Lopez-Lopez MT, Zugaldia A, Gomez-Ramirez A, Gonzalez-Caballero F, Duran JDG (2008b) Effect of
615 particle aggregation on the magnetic and magnetorheological properties of magnetic
616 suspensions. *J Rheol* 52: 901-912. <https://doi.org/10.1122/1.2931008>

617 Machovsky M, Mrlik M, Kuritka I, Pavlinek V, Babayan V (2014) Novel synthesis of core-shell urchin-
618 like ZnO coated carbonyl iron microparticles and their magnetorheological activity. *RSC Adv* 4:
619 996-1003. <https://doi.org/10.1039/c3ra44982c>

620 Machovsky M, Mrlik M, Plachy T, Kuritka I, Pavlinek V, Kozakova Z, Kitano T (2015) The enhanced
621 magnetorheological performance of carbonyl iron suspensions using magnetic Fe₃O₄/ZHS
622 hybrid composite sheets. *RSC Adv* 5: 19213-19219. <https://doi.org/10.1039/c4ra14054k>

623 Marins JA, Plachy T, Kuzhir P (2019) Iron-sepiolite magnetorheological fluids with improved
624 performances. *J Rheol* 63: 125-139. <https://doi.org/10.1122/1.5048051>
625 Matyjaszewski K (2012) Atom transfer radical polymerization (ATRP): Current status and future
626 perspectives. *Macromolecules* 45: 4015-4039. <https://doi.org/10.1021/ma3001719>
627 Morillas JR, Bombard AJF, de Vicente J (2018) Magnetorheology of bimodal fluids in the single-
628 multidomain limit. *Ind Eng Chem Res* 57: 13427-13436.
629 <https://doi.org/10.1021/acs.iecr.8b03438>
630 Park BJ, Fang FF, Choi HJ (2010) Magnetorheology: materials and application. *Soft Matter* 6: 5246-5253.
631 <https://doi.org/10.1039/c0sm00014k>
632 Park DE, Chae HS, Choi HJ, Maity A (2015) Magnetite-polypyrrole core-shell structured microspheres
633 and their dual stimuli-response under electric and magnetic fields. *J Mater Chem C* 3: 3150-
634 3158. <https://doi.org/10.1039/c5tc00007f>
635 Park DE, Choi HJ, Vu CM (2016) Stimuli-responsive polyaniline coated silica microspheres and their
636 electrorheology. *Smart Materials and Structures* 25: 11. [https://doi.org/10.1088/0964-
637 1726/25/5/055020](https://doi.org/10.1088/0964-1726/25/5/055020)
638 Parsian M, Mutlu P, Yalcin S, Tezcaner A, Gunduz U (2016) Half generations magnetic PAMAM
639 dendrimers as an effective system for targeted gemcitabine delivery. *International Journal of*
640 *Pharmaceutics* 515: 104-113. <https://doi.org/10.1016/j.ijpharm.2016.10.015>
641 Plachy T, Kutalkova E, Sedlacik M, Vesel A, Masar M, Kuritka I (2018) Impact of corrosion process of
642 carbonyl iron particles on magnetorheological behavior of their suspensions. *J Ind Eng Chem*
643 66: 362-369. <https://doi.org/10.1016/j.jiec.2018.06.002>
644 Roupec J, Mazurek I (2011) Stability of magnetorheological effect during long term operation. Springer-
645 Verlag Berlin, Berlin
646 Roupec J, Mazurek I, Strecker Z, Klapka M (2013) The behavior of the MR fluid during durability test.
647 In: Unal HI (ed) 13th International Conference on Electrorheological Fluids and
648 Magnetorheological Suspensions, vol 412. Iop Publishing Ltd, Bristol
649 Sedlacik M, Pavlinek V (2014) A tensiometric study of magnetorheological suspensions' stability. *RSC*
650 *Adv* 4: 58377-58385. <https://doi.org/10.1039/c4ra11842a>
651 Seo YP, Han S, Choi J, Takahara A, Choi HJ, Seo Y (2018) Searching for a stable high-performance
652 magnetorheological suspension. *Adv Mater* 30: 13. <https://doi.org/10.1002/adma.201704769>
653 Ulicny JC, Balogh MP, Potter NM, Waldo RA (2007) Magnetorheological fluid durability test - Iron
654 analysis. *Mater Sci Eng A-Struct Mater Prop Microstruct Process* 443: 16-24.
655 <https://doi.org/10.1016/j.msea.2006.06.050>
656 Utami D, Ubaidillah, Mazlan SA, Imaduddin F, Nordin NA, Bahiuddin I, Aziz SAA, Mohamad N, Choi SB
657 (2018) Material characterization of a magnetorheological fluid subjected to long-term
658 operation in damper. *Materials* 11: 17. <https://doi.org/10.3390/ma11112195>
659 Volkova O, Bossis G, Guyot M, Bashtovoi V, Reks A (2000) Magnetorheology of magnetic holes
660 compared to magnetic particles. *J Rheol* 44: 91-104. <https://doi.org/10.1122/1.551075>
661 Yang YB, Li L, Chen G (2009) Static yield stress of ferrofluid-based magnetorheological fluids. *Rheol*
662 *Acta* 48: 457-466. <https://doi.org/10.1007/s00397-009-0346-z>
663 Yin JB, Wang XX, Zhao XP (2015) Silicone-grafted carbonaceous nanotubes with enhanced dispersion
664 stability and electrorheological efficiency. *Nanotechnology* 26: 9.
665 <https://doi.org/10.1088/0957-4484/26/6/065704>
666 Zhang P, Dong YZ, Choi HJ, Lee CH (2018) Tribological and rheological tests of core-shell typed carbonyl
667 iron/polystyrene particle-based magnetorheological fluid. *J Ind Eng Chem* 68: 342-349.
668 <https://doi.org/10.1016/j.jiec.2018.08.005>
669 Zhu XC, Jing XJ, Cheng L (2012) Magnetorheological fluid dampers: A review on structure design and
670 analysis. *J Intell Mater Syst Struct* 23: 839-873. <https://doi.org/10.1177/1045389x12436735>

671